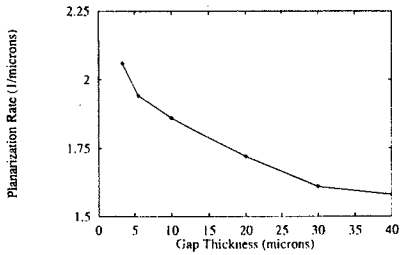

Fig. 9. Planarization rate as a function of hydrodynamic layer thickness using two-parameter erosion model.

that increased selectivity is possible through decreasing the hydrodynamic layer thickness. However, pad feature size and pad deformation may affect the model accuracy for smaller gaps.[1]

The variation of planarization rates with pattern density is important to understand since it leads to a polishing process that is wafer dependent. The pattern density study here simulates erosion of a square wave by setting l_2 = 0.4 μm and $l_1 = l_2$. The selectivity varies in a way similar to those in Fig. 8 allowing the computation of planarization rates which are shown in Fig. 10. Although the feature sizes considered here are significantly smaller than those considered in Ref. 17, the behavior of the planarization rate with feature width qualitatively agrees with those experimental results.

Conclusion

Because CMP involves several mechanisms on distinct geometric scales, various models and experimental methods must be developed and linked to establish a complete understanding. The feature-scale model described here, which is for processes utilizing a hydrodynamic slurry layer, has demonstrated the capability of linking wafer- and particle-scale models together through the layer thickness (h) and the erosion law (V_n). For the particular layer thickness used here in comparisons to experimental data, the two-parameter form of V_n is an erosion law that provides good prediction of erosion profiles over various shapes.

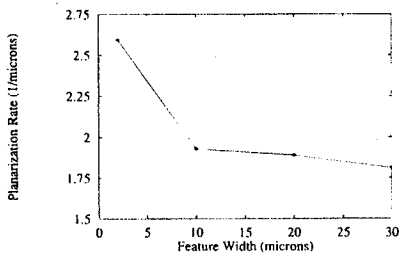

Fig. 10. Planarization rate as a function of feature width using two-parameter erosion model.

The increased understanding of the mechanics obtained from a feature-scale model can be used to evaluate the effects of various process parameters. For example, the dependence of the hydrodynamic layer on polishing rotation speed, wafer curvature and slurry viscosity[3] can be used to link these process parameters to the feature erosion profiles and planarization rates. In a similar way, the chemical properties associated with various slurries can be implemented in continuum erosion laws to test their effects. Thus, the type of physics-based modeling demonstrated here has the potential not only for increasing understanding, but also for optimizing the polishing process.

Acknowledgment

Special thanks to Jim Warnock at IBM for supplying the experimental erosion profile data files. Also thanks to Anthony Toprac and Roger Hill for proofreading the manuscript. The fluid flow solutions were obtained using the program Free-Flow, which was developed as part of this work.

Manuscript submitted Oct. 18, 1993; revised manuscript received Feb. 7, 1994.

SEMATECH assisted in meeting the publication costs of this article.

REFERENCES

1. L. Cook, *J. Non-Cryst. Solids*, **120**, 152 (1990).
2. G. M. Bartenev and V. V. Lavrentev, *Friction and Wear of Polymers*, p. 30, Elsevier Scientific Publishing Co., New York (1981).
3. S. R. Runnels and L. M. Eyman, *This Journal*, **141**, 1698 (1994).
4. K. Akamatsu, T. Nakamura, and N. Arakawa, *Bull. Japan Soc. Prec. Eng.*, **19**, 120 (1985).
5. J. Warnock, *This Journal*, **138**, 2398 (1991).
6. R. Shultz, J. Currie, and A. Ticknor, U.S. Pat. 5,267,418 (1993).
7. E. Banks, U.S. Pat. 4,256,535 (1981).
8. S. Timoshenko and J. Goodier, *Theory of Elasticity*, p. 12, McGraw-Hill, New York (1934).
9. I. G. Currie, *Fundamental Mechanics of Fluids*, p. 3, McGraw-Hill, New York (1974).
10. R. Panton, *Incompressible Flow*, p. 638, John Wiley & Sons, New York (1984).
11. G. F. Carey and J. T. Oden, *Finite Elements: Fluid Mechanics*, p. 115, Prentice-Hall, Englewood Cliffs, NJ (1986).
12. P. Hood, *Int. J. Numer. Methods Eng.*, **10**, 379 (1976).
13. N. Kikuchi and Y. Ichikawa, *ibid.*, **14**, 1221 (1979).
14. R. D. Davies, P. B. Arnell, and T. L. Whomes, *Tribology Principles and Design Applications*, p. 124, Springer-Verlag, New York (1991).
15. F. Preston, *J. Soc. Glass Technol.*, **11**, 247 (1927).
16. S. Runnels and J. Warnock, Private communication (1993).
17. M. Thomas, P. Renteln, and J. Pierce, in *VMIC Conference June 1990*, p. 57, IEEE, New York (1990).

The Role of Reactive Elements on Scale Growth in High-Temperature Oxidation of Pure Nickel, Iron, Cobalt, and Copper

I. Oxidation Kinetics and Scale Morphology

Anna Strawbridge* and Robert A. Rapp**

Department of Materials Science and Engineering, The Ohio State University, Columbus, Ohio 43210

ABSTRACT

Recently, Pieraggi and Rapp proposed the "poisoned interface" model, as a novel interpretation for the reactive-element effect (REE) in chromia-forming alloys; the mechanism should also be applicable to any other scaling reaction involving a cation-diffusing scale and a suitable impurity segregant. The premise of the current study was that the relative size of the ions involved is an important factor in producing the required interfacial segregation by the reactive element. The high-temperature oxidation kinetics and morphologies were studied for pure Ni, Co, Fe, and Cu coupons coated with thin superficial films (100 to 500 Å) of Ca, Sr, or Ba introduced by vacuum evaporation. In every case, the modified coupons showed a reduction in scaling rate compared to unmodified coupons, and there was a noticeable change in oxide morphology. At 850°C, 250 Å of initially deposited Ca on pure Ni effected a reduction in the parabolic rate constant for Ni by a factor of 20. These results provide preliminary evidence which is consistent with the "poisoned interface" interpretation for the REE.

The action of reactive elements in improving the oxidation resistance of chromia- and alumina-forming alloys is a popular, important, and controversial subject. Extremely small amounts of certain reactive elements (*e.g.*, Y, Ce, La, and Zr) or a dispersion of their oxides drastically and favorably affect the growth of scales on certain high-temperature alloys. Extensive investigations have been carried out, and numerous theories have been put forward to explain the reactive element effect (REE), as reviewed by several authors.[1-4] Consistent with the reviews, the existing interpretations for the REE do not provide comprehensive explanations for the observed effects.[5]

In alumina-formers, the only significant effect of reactive elements seems to be an improvement in scale adhesion. Several authors[6-8] have credited the action of the reactive element in alumina-forming alloys to eliminating sulfur segregation at the alloy/scale interface, thereby leading to improved scale adherence (the "sulfur effect").

For the growth of a chromia protective scale on an iron-, nickel-, or cobalt-base alloy, the following effects have been demonstrated: (*i*) scale adherence is greatly improved, (*ii*) the parabolic scaling rate constant is reduced significantly, sometimes by a factor of 10 or more, (*iii*) a lower concentration of chromium is adequate to form a protective chromia scale, and (*iv*) the dominant scale-growth mechanism is changed from scale growth at the oxide/gas interface resulting from dominant outward cation diffusion (*via* grain boundaries and other short circuits), to scale growth at the alloy/scale interface resulting from inward diffusion of oxygen anions (also *via* short-circuit routes).

Among the suggested mechanisms for the REE in chromia-forming alloys, segregation of the reactive element to oxide grain boundaries leading to inhibited diffusion of chromium ions and enhanced oxygen diffusion enjoys some acceptance based on studies by Przybylski *et al.*[9] and Cotell *et al.*[10]

Recently, Pieraggi and Rapp[5] proposed the "poisoned interface" model as a novel interpretation for the REE for chromia growth on alloys; this model is consistent with the four known characteristics of the REE. According to an earlier paper,[11] for the growth of cation-diffusing scales (*e.g.*, undoped chromia), the climb into the metal of some fraction of the interfacial misfit edge dislocations at the metal/scale interface and their subsequent glide back to the interface (see Fig. 1), annihilates cation vacancies (or creates interstitial cations) to support cation-vacancy diffusion in the scale. If cation-vacancy annihilation (or interstitial-cation creation) is prevented for some reason, then scale growth by cation diffusion cannot occur. In the poisoned-interface model,[5] the relatively large, highly charged reactive element ions segregate to and immobilize (pin) the interfacial misfit dislocations (as shown in Fig. 2). Thus, if the climb of the misfit dislocations at the metal/scale inter-

* Electrochemical Society Student Member.
** Electrochemical Society Fellow.

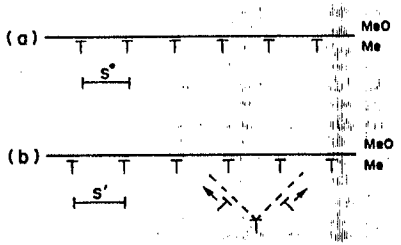

Fig. 1. Schematic illustration of mechanism to effect vacancy annihilation in cation-diffusing scales: (a) Misfit dislocations at metal/scale interface with equilibrium separation $s°$. (b) Climb of misfit dislocations into metal and subsequent glide back to the interface, resulting in separation s'.

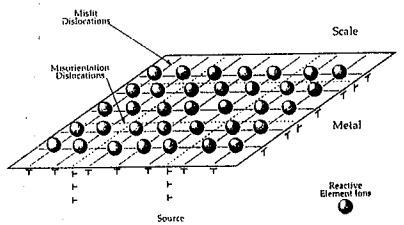

Fig. 2. Schematic representation of the "poisoned-interface" interpretation of the REE. Large, highly charged reactive element ions segregate to metal/scale interface, thereby pinning the misfit dislocations and preventing scale growth by cation diffusion.[5]

Table I. Ionic radius ratios for systems involving a chromia scale and various reactive elements. Ionic radii from Ref. 13.

RE ionic radii (Å)	Comparison with Cr^{3+} (r = 0.63 Å) $R = r_{RE}/r_{Cr}$
Y^{3+} (0.893)	1.42
Ce^{3+} (0.92)	1.46
La^{3+} (1.016)	1.61
Th^{4+} (1.02)	1.62

face were sufficiently blocked by the pinning action of the reactive-element ions, scale growth by cation diffusion could be prevented, and growth would then proceed by oxygen diffusion *via* anion vacancies (or interstitials).[5] Scale growth supported by anion diffusion could occur by the lateral climb of misorientation dislocations in the oxide at the metal/scale interface,[9-12] even for a segregated interface.

The poisoned interface mechanism should, in principle, be applicable to any metal or alloy provided with a suitable interfacial segregant, in any oxidant (*e.g.*, oxygen or sulfur), which leads to the formation of a cation diffusing scale (*e.g.*, NiO on nickel). In the present study, it is postulated that the relative size of the reactive ion is important in deciding the interfacial bond of this segregant to the interface and effecting the REE. Table I shows the ionic-radius ratio ($R = r_{RE}/r_{Cr}$) for systems involving a chromia scale and reactive elements known to be effective in improving oxidation resistance. These ion sizes[13] are based on six-fold coordination with surrounding anions, which does not correspond directly to their geometry at a segregated interface. While ion sizes are known to depend upon their specific coordination, the present use of the radii for CN = 6 seems suitable for comparison of relative ion size for similar elements.

From the literature, the most dramatic demonstration of the REE in alloys has been shown for additions of yttrium or cerium (or their oxides) into chromia-forming alloys or onto their surfaces (R = 1.42 and 1.46, respectively). The REE has also been produced for pure chromium with yttrium (or other reactive elements) as an alloy addition,[14] and otherwise with implanted yttrium,[7] or with Y_2O_3,[15] La_2O_3,[16] or ThO_2[17] dispersions. However, for the oxidation of pure nickel with additions of, for instance, yttrium[18-22] (R = 1.29) or cerium[22-25] (R = 1.33), the full REE is often not apparent, with the oxidation rate being increased by the dopant under many conditions. Therefore, one can propose that for favorable interfacial segregation, resulting in the effective pinning of misfit dislocations, the ionic radius ratio of the system must be relatively high, in the range 1.4 to 1.6. By this criterion, any given elements, *e.g.*, yttrium or cerium, may not necessarily be expected to cause the REE generally for most scaling reactions.

Table II. Ionic radius ratios for pure metals (which produce cation-diffusin oxide scales) with large ion impurities. Combinations selected to produce a ratio in the range 1.4 to 1.6. Ionic radii from Ref. 13.

Ionic radii (Å)	Ratio of ionic radii (R) Ni^{2+} (0.69)	Co^{2+} (0.72)	Fe^{2+} (0.74)	Cu^{+} (0.96)
Gd^{3+} (0.938)	1.36			
Np^{3+} (0.95)	1.38			
Eu^{3+} (0.95)	1.38			
Sm^{3+} (0.97)	1.41			
Na^{+} (0.97)	1.41			
U^{3+} (0.97)	1.41			
Pm^{3+} (0.979)	1.42			
Ca^{2+} (0.99)	1.44[a]	1.38[a]	[a]	[a]
Nd^{3+} (0.995)	1.44	1.38		
Th^{4+} (1.02)	1.48	1.42	1.38	
La^{3+} (1.061)	1.54	1.47	1.43	
Sr^{2+} (1.12)	[a]	1.56[a]	1.51[a]	[a]
Ac^{3+} (1.18)			1.60	
K^{+} (1.33)				1.39
Ba^{2+} (1.34)	[a]	[a]	[a]	1.40[a]
Rb^{+} (1.47)				1.53

[a] Chosen for study here.

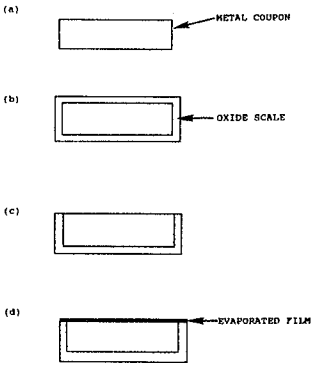

Fig. 3. Schematic diagram of the stages in sample preparation (coupon shown in cross section):[32] (a) Metal coupon. (b) Metal coupon after preoxidation to form a thick blocking scale on all faces. (c) Blocking scale removed from one large face. (d) Thin film of alkaline earth metal evaporated onto exposed metal surface.

Limited studies in the literature, involving oxidation studies of pure metals which form cation-diffusing scales implanted with various metals, do in fact correlate somewhat with the ionic radii requirement postulated above. For instance, Collins *et al.*[26] found that implants of lanthanides into chromium resulted in considerable inhibition of oxidation at 750°C in O_2 for 30 min, while other elements, in general of smaller ionic radii, caused less effect. Also, in a study of implants into pure nickel for oxidation at 630°C in O_2,[27] relatively large ions (Ca, Bi, Ce) led to a reduced oxidation rate while other (smaller) elements increased the oxidation rate.

To cause the REE, in addition to having a relatively large ionic radius, the additive element must have a higher oxygen affinity than the base metal of the substrate. Iron with a bismuth implant might be expected to cause some reduction in oxidation due to an ionic radius ratio of 1.3, but due to the low oxygen affinity of bismuth, there is no effect on iron oxidation at >600°C.[28] Also, a reduction in oxidation rate may be produced by impurity elements, independent of the ionic radii, due to other mechanisms. For instance, a protective oxide layer may form (*e.g.*, for aluminum implanted in iron oxidized at 447 to 747°C),[29] or the scale may

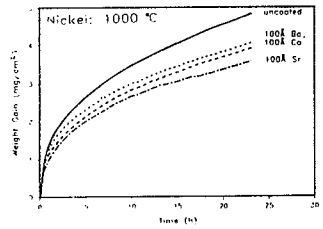

Fig. 4. Weight gain with time for oxidation in 1 atm O_2 at 1000°C of pure Ni coupons with and without a 100 Å coating of Ba, Ca, or Sr.

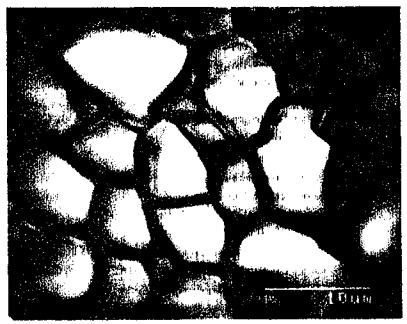

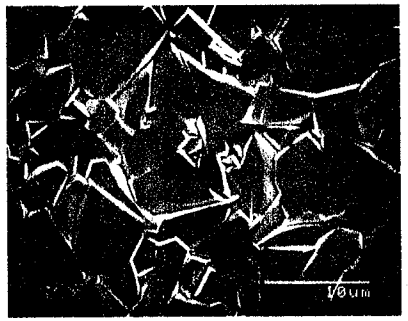

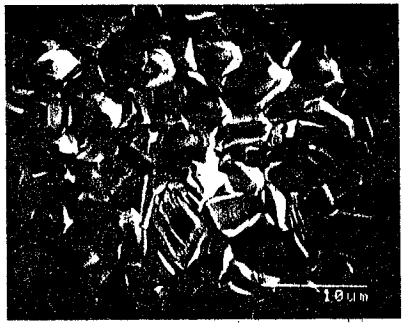

Fig. 5. Scanning electron micrographs of the surface of the scale formed on pure Ni coupons after oxidation in 1 atm O_2 at 1000°C for 24 h: (a, top left) Uncoated Ni; (b, above) Ni/100 Å Ca; (c, left) Ni/250 Å Ca.

be electrically doped (*e.g.*, for lithium implanted into nickel),[31] or fast diffusion paths (grain boundaries) may be blocked by the impurity (*e.g.*, for bismuth implants in iron at temperatures <600°C[28] and ceria coatings on nickel oxidized at 900°C).[24] Therefore, for demonstration of the poisoned-interface model, the impurity elements must be chosen carefully.

The purpose of the present study was to provide some experimental evidence to test the generality of the poisoned-interface model, even for extreme examples of rapidly oxidizing pure metals which form cation-diffusing scales. Table II presents the ionic radii for a wide range of quite stable cations and the ratios of their radii to those for nickel, cobalt, iron, and copper. Depending on the particular metal, certain large ions exhibit ion radius ratios (R) in the range 1.4 to 1.6. The superficially introduced impurities chosen for this study were the alkaline earth metals (barium, calcium, and strontium), which are highly oxygen active and for which there is at least one metal/impurity combination giving R in the range predicted for effective segregation. Thin films (100 to 500 Å) of the alkaline earth metals were deposited onto pure metal coupons by vacuum evaporation, and thermogravimetric measurements were performed in pure, dry oxygen at temperatures in the range 500 to 1000°C (depending on the metal substrate). Specimens were characterized by scanning electron microscopy (SEM) and optical microscopy. In a future publication, chemical analysis by secondary-ion mass spectrometry (SIMS) will be presented.

Experimental Procedure

Preparation and preoxidation of metal coupons.—Thick coupons were cut from high-purity nickel rod (99.998%, Materials Research Corp.), cobalt rod (99.998%, Materials Research Corp.), cold-rolled copper (OFHC grade, >99.95%, Williams & Co.), and iron pieces (electrolytic, 99.98%, Johnson-Matthey). The nickel and cobalt disks were approximately 12 mm in diam and 1 mm thick, and the iron and copper coupons were approximately 10 × 10 × 1 mm. A 1 mm diam hole was drilled near the edge of each coupon, and then all sides were ground by 600 grit SiC. The coupons were annealed in purified argon for 4 h at 1050°C for nickel, 950°C for cobalt, 850°C for iron, and 750°C for copper. After annealing, the surfaces were lightly reground to 600 grit SiC, and each sample was weighed, measured, and degreased.

The alkaline earth metals were evaporated onto one large surface of each coupon only, after a specific preoxidation treatment. Following a suggestion by Pieraggi,[32] to enable an accurate determination of scaling kinetics on the modified surface, significant scale growth on all other sides of the coupon was avoided by preoxidizing the coupons to form thick, adherent oxide scales. The steps in coupon preparation are shown in Fig. 3. Prior to vacuum evaporation of the "reactive elements," the coupons were oxidized at high temperatures for extended durations in 1 atm pure oxygen to produce scales on the order of 100 µm thick. This scale was removed from one main face of each coupon by grinding on SiC papers, and the exposed metal surface was further polished by 1 µm diamond paste and ultrasonically cleaned in preparation for evaporative deposition. During subsequent oxidation study, the thick prior scales showed minimal growth, but the global kinetics were nevertheless corrected for this minor weight gain.

Deposition of alkaline earth metals by vacuum evaporation.—The source materials for evaporation of thin films were pieces of pure calcium, strontium, and barium (pro-

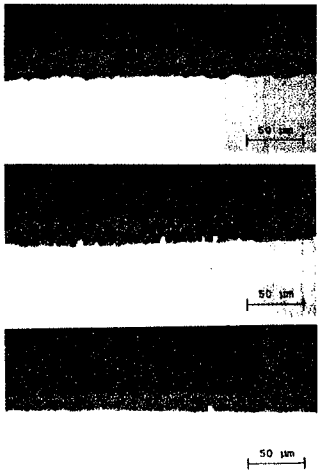

Fig. 6. Optical micrographs of cross sections of NiO scales formed on pure Ni coupons after oxidation in 1 atm O_2 at 1000°C for 24 h: (a, top) Uncoated Ni; (b, center) Ni/100 Å Ca; (c, bottom) Ni/250 Å Ca.

vided by Superconductive Components, Inc.), from which small pieces were cut. Thin films of these metals were deposited onto the polished faces of the substrates by thermal

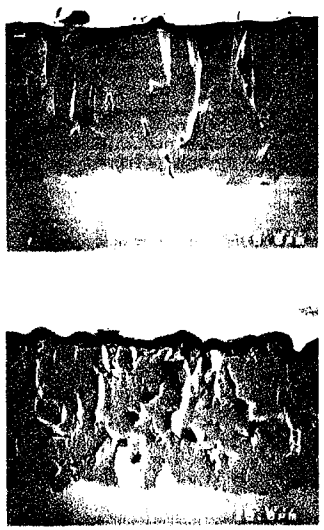

Fig. 7. Scanning electron micrographs of cross sections of scales formed on pure Ni coupons after oxidation in 1 atm O_2 at 1000°C for 24 h: (a, top) Uncoated Ni; (b, bottom) Ni/100 Å Ba.

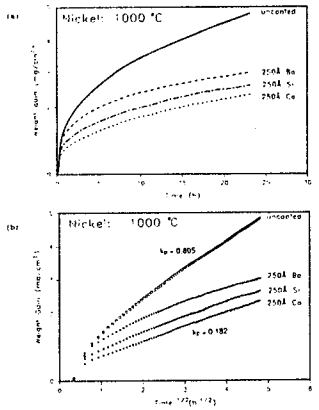

Fig. 8. Oxidation kinetics for pure Ni coupons with and without 250 Å films of Ba, Ca, and Sr, in 1 atm O_2 at 1000°C: (a) Weight gain with time, (b) Pieraggi plot.

evaporation and condensation in a high vacuum (in the range 10^{-3} Pa). During evaporation of the films, the nickel, cobalt, and iron coupons were held horizontally, above the vapor source, by small magnets on a steel sheet; the copper samples were held by a small amount of vacuum grease (subsequently removed using acetone). An electrically heated tungsten boat contained the required source metal. Alkaline earth metals are particularly liable to atmospheric deterioration and so, to ensure minimum contamination, the metals were degassed (by heating in the vacuum at low temperature) until the pressure in the chamber was sufficiently low and steady; then the substrates were exposed to the evaporant.

The thickness of the films was controlled by use of a quartz crystal oscillator. Films were deposited to 100, 250,

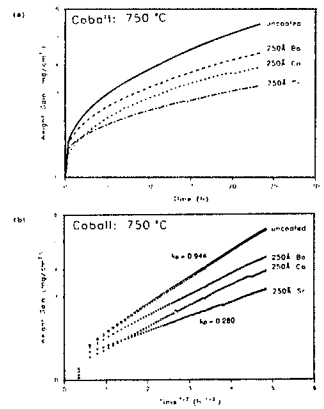

Fig. 9. Oxidation kinetics for pure Co coupons with and without 250 Å films of Ba, Ca, and Sr, in 1 atm O_2 at 750°C: (a) Weight gain with time, (b) Pieraggi plot.

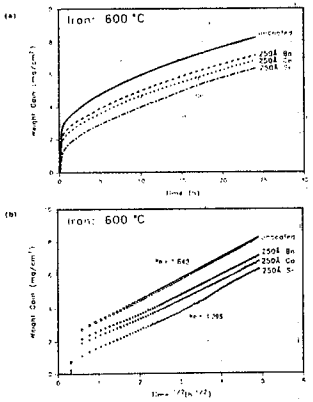

Fig. 10. Oxidation kinetocs for pure Fe coupons with and without 250 Å films of Ba, Ca, and Sr, in 1 atm O_2 at 600°C: (a) Weight gain with time; (b) Pieraggi plot.

or 500 Å in thickness and at a deposition rate of approximately 10 Å/s. Coating by evaporation has been widely studied, and for increasing amounts of deposit, the deposit structure changes from islands to lacunar (porous network) to quasicontinuous. A study by Guadart *et al.*[33] of vacuum-evaporated deposits of barium, calcium, and strontium on a plane quartz substrate showed that relatively thick islands of metal formed at low mass thickness of deposit, and the layers approached continuity at 20, 70, and 300 Å mass thickness, respectively. The films deposited in this study, with the possible exception of the 100 Å films, should therefore provide complete coverage of the substrate.

To minimize contamination of the films on removal from the evaporation unit, the vacuum chamber was brought to atmospheric pressure by flushing with pure, dry oxygen. In this way the highly reactive metal films were likely con-

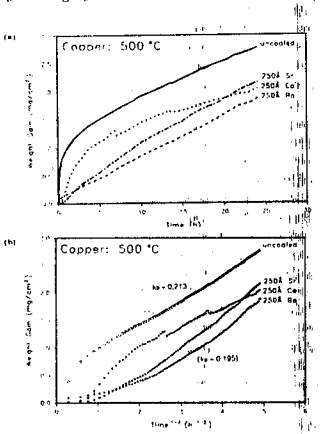

Fig. 11. Oxidation kinetics for pure Cu coupons with and without 250 Å films of Ba, Ca, and Sr, in 1 atm O_2 at 500°C: (a) Weight gain with time, (b) Pieraggi plot.

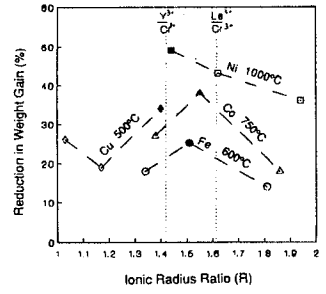

Fig. 12. Trends in reduction in weight gain (compared to uncoated samples) after oxidation in 1 atm O_2 for 24 h for pure metals with evaporated coatings of 250 Å Ba, Ca, or Sr. Oxidation at 1000°C for Ni, 750°C for Co, 600°C for Fe, and 500°C for Cu. Ionic radius ratio, $R = r_{RE}/r_{metal}$.

converted to films of pure oxide. The samples were stored in a desiccator until required for subsequent oxidation tests.

Oxidation studies.—Oxidation of coupons (with and without thin alkaline earth metal/oxide films) was carried out in a thermogravimetric analyzer (Cahn TG-171), with a balance sensitivity to 1 μg. The coupons were suspended by platinum wire, and oxidized in pure, dry, flowing oxygen at 1 atm for 24 h at 1000°C for nickel, 750°C for cobalt, 600°C for iron, and 500°C for copper. These differing oxidation temperatures were chosen so that the four substrate metals exhibited comparable parabolic oxidation kinetics. Some additional tests on nickel were carried out at 850°C for 48 h.

After oxidation, the oxide-scale surfaces and the sample cross sections were observed by scanning electron microscopy (SEM) and optical microscopy.

Results and Discussion

100 Å films on nickel.—Figure 4 shows the weight-gain kinetics at 1000°C for uncoated nickel and for nickel coated with 100 Å alkaline earth metal (oxide). All the coated cou-

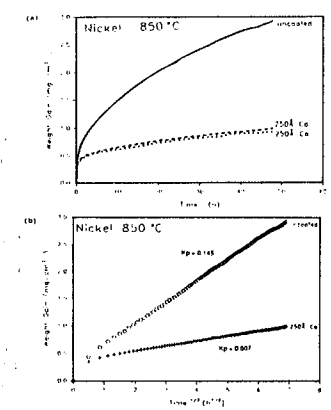

Fig. 13. Oxidation kinetics for pure Ni coupons with and without 250 Å films of Ca, in 1 atm O_2 at 850°C: (a) Weight gain with time; (b) Pieraggi plot.

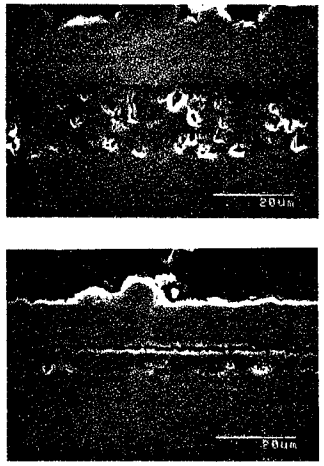

Fig. 14. Scanning electron micrographs of cross sections of NiO scales formed on pure Ni coupons after oxidation in 1 atm O_2 at 850°C for 48 h: (a, top) Uncoated Ni; (b, bottom) Ni/250 Å Ca.

pons showed a reduction in oxidation rate, with the strontium coating causing the greatest effect at about 20% reduction in final weight gain.

The surface of the NiO scale produced on pure nickel consisted of nominally round grains, with an average dimension of about 10 μm (see Fig. 5a). For the scales formed on coated coupons, the morphology was quite different, in that the grains were irregular, angular, and of smaller average dimension (about 5 μm), as shown in Fig. 5b for the calcium-coated coupon.

Cross-sectional examination revealed that the thicknesses of the NiO scales were comparable, approximately 30 μm, but the uncoated and the coated samples differed notably in scale structure and the nature of the metal/scale interface. For uncoated nickel (see Fig. 6a), the metal/scale interface is essentially plane; however, for the three coated coupons, the interfaces were irregular with frequent, abrupt steps (see Fig. 6b for the calcium-coated sample). In some cases, faster scale growth next to steps led to encapsulation of nickel islands in the NiO scale. The reduction in the oxidation rate of the coated samples, shown in Fig. 4, thus appears to result from localized areas of reduced oxidation.

The SEM observation of scale cross sections, as seen in Fig. 7a, showed that the outermost scale produced on uncoated nickel consisted predominantly of columnar grains with an equiaxed grain layer adjacent to the metal. The coated samples produced a different morphology (shown in Fig. 7b for barium-coated nickel) which consisted possibly of two layers of small grains, with many of those in the outer layer being elongated perpendicular to the scale surface. Figure 7b also shows an interfacial step, at a site of localized blocking of scale growth.

The poisoned interface model requires that the array of interfacial misfit dislocations be pinned, by segregated reactive element ions, which may require less than a monolayer of dopant at the interface. In this respect, a 100 Å film of a suitable reactive element on the substrate surface could be sufficient to cause a "full" REE.[12] A full REE implies that the interfacial step involving cations and vacancies is totally blocked, so that anion diffusion dominates. Incomplete interfacial segregation would lead to only partial blocking of the interfacial cation/vacancy step, which may be the result caused by the 100 Å film deposits in this study (for oxidation at quite high temperatures). The nonuniform nature of the vacuum evaporation deposition process can result in full surface coverage not being achieved for such thin films,[33] and therefore thicker films were deposited for all other experiments to achieve a uniform effect. If the reactive elements were applied by a more uniform method, *e.g.*, sputtering or ion implantation, then a lesser amount of deposition could probably suffice to cause a full REE. Indeed, Hussey *et al.*[35] demonstrated a full REE by 4 nm CeO_2 coatings sputtered onto the surface of Fe-25%Cr, after oxidation at 1100°C at $P_{O_2} = 10^{-3}$ atm.

250 Å films on nickel, cobalt, iron, and copper.—Oxidation kinetics.—Figure 8a shows the scaling kinetics at 1000°C for uncoated nickel and for samples coated with 250 Å of barium, calcium, or strontium. The 250 Å coatings were much more effective in reducing oxidation than the 100 Å coatings on nickel at the same temperature. Calcium caused the greatest effect of the 250 Å films deposited. The parabolic plot, after Pieraggi,[34] of Fig. 8b shows that scale growth is approximately parabolic in each case and that the maximum reduction in the parabolic rate constant (k_p) is approximately 80%.

Figures 9 to 11 show similar plots for the uncoated and coated cobalt at 750°C, iron at 600°C, and copper at 500°C, respectively. In every case, a 250 Å coating led to a reduction in scale growth compared to the respective uncoated coupons. Similar to nickel, the kinetics for the coated and uncoated cobalt and iron were parabolic, with the largest reduction in k_p resulting for 250 Å strontium in each case: a reduction by 70% for cobalt and by 15% for iron. For the iron coupons, the oxidation rate constant was reduced only slightly, but due to differences in the degree of initial oxidation there was a greater reduction in the final weight gain (−30%). The most effective dopant for copper was barium, and as can be seen in Fig. 11, the final weight-gain was reduced by approximately 35%. Also, the kinetic behavior changed noticeably from parabolic for the uncoated coupon to paralinear for the modified surface, indicating a departure from diffusion-controlled scaling.

The most effective combinations of base metal and 250 Å coating at the temperatures studied were Ni/Ca, Co/Sr, Fe/Sr, and Cu/Ba. Figure 12 is a plot of percent reduction in weight gain after 24 h *vs.* ion-radius ratio ($R = r_{RE}/r_{metal}$). The most effective combinations (filled-in points) have R values closest to 1.5, and are therefore comparable to the values for the most effective reactive elements in oxidation of chromium and chromia-forming alloys (*e.g.*, $Y^{3+}/Cr^{3+} = 1.42$, $La^{3+}/Cr^{3+} = 1.61$ as indicated by dotted lines in Fig. 12). However, on each side of the 1.4 to 1.6 range, the coated coupons still showed some reduction in oxidation rate compared to uncoated coupons. These observations were interpreted to indicate that the large ions preferentially segregated to the reactive sites (misfit edge dislocations) at the metal/scale interface, consistent with the poisoned interface model.[5] Also, there seemed to be an optimum size for the segregant ion (depending on the oxidized metal), which was suitable for efficient pinning of the dislocation array.

Since many studies of the REE have shown that the effect is more pronounced at lower temperatures, oxidation was carried out for nickel and nickel coated with 250 Å calcium at 850°C for 48 h. These experimental conditions were also used for a reproducibility test, which provided the kinetics shown in Fig. 13. For 850°C, the calcium-coated coupons showed a substantial reduction in oxidation, and the parabolic rate constant was reduced by a factor of 20. Figure 13 also shows that the greatly reduced kinetics for the two calcium-coated samples were almost identical, demonstrating good reproducibility for the method.

The 250 Å calcium coatings on nickel had a much greater effect on the oxidation at 850°C than at 1000°C. Impurity segregation is exothermic, and therefore enhanced interfacial enrichment occurs at a lower temperature. Impurities may be drained from the interface at higher temperatures, through an entropy-of-mixing term, because the minor solubility of the impurity ions into the metal substrate and into the scale increase with temperature. Recently, Pint and Hobbs[36] found (by STEM sputter depth profiling) enrichment of the reactive element near the scale/gas interface for oxidation of α-alumina-formers in 1 atm O_2 at 1000 to 1500°C. The explanation given for this was that the reactive element diffused towards the higher oxygen potential. An alternative interpretation would be that demixing of the multicomponent scale occurred in the oxygen potential gradient.[37] In either case, this increase in the enrichment would be expected at higher temperatures due to increased mobility of the reactive element in the scale.

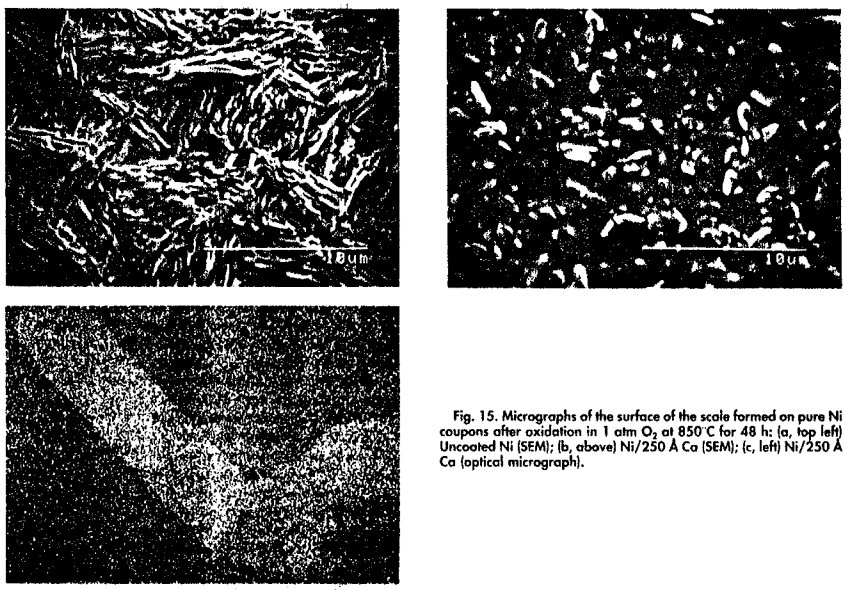

Fig. 15. Micrographs of the surface of the scale formed on pure Ni coupons after oxidation in 1 atm O_2 at 850°C for 48 h: (a, top left) Uncoated Ni (SEM); (b, above) Ni/250 Å Ca (SEM); (c, left) Ni/250 Å Ca (optical micrograph).

Scale morphology.—The surface morphologies of oxide grains for the various 250 Å coated nickel coupons after oxidation at 1000°C were similar (shown for calcium-coated nickel in Fig. 5c), being somewhat angular in shape and showing irregularities (*e.g.*, striations and protrusions). Cross sections showed that the total scale thicknesses were 16, 22, and 20 μm for calcium-, barium-, and strontium-coated coupons, respectively, compared to 30 μm on uncoated nickel. For the 250 Å calcium-coated coupon there were occasional interfacial "steps" (see Fig. 6c), as seen frequently for all the 100 Å coated samples, but for the 250 Å barium- and strontium-coated coupons, the metal/scale interface was smooth. Therefore, it was concluded that the reduction in scaling rate resulted from uniformly inhibited growth of the scale along the interface.

For oxidation at 850°C, the uncoated nickel produced a NiO scale approximately 18 μm thick (Fig. 14a). The scale on the 250 Å calcium-coated nickel had a smaller grain size and was nonuniform in thickness, ranging from 2 to 8 μm, due to an irregular metal/scale interface (Fig. 14b). The external scale surfaces were substantially different, with those on uncoated nickel being small and elongated (Fig. 15a) and those on 250 Å calcium-coated nickel being rounded and densely packed (Fig. 15b). Observation of the oxidized, calcium-coated nickel coupon in plan revealed the outline of the grain structure of the underlying metal, as shown in the optical micrograph of Fig. 15c, which is strong evidence for scale growth by anion diffusion.

Figure 16 shows the surface morphologies of the scales formed on uncoated cobalt and the most effective coated sample (250 Å strontium) after oxidation at 750°C. The grains on the strontium-coated coupon are considerably smaller, and the metal/oxide interface on the strontium-coated coupon is more uniform. A cross section of the uncoated cobalt coupon (see Fig. 17a) shows that a thick layer (28 μm) of CoO forms adjacent to the metal, with a thinner outer layer (12 μm) of Co_3O_4. On the strontium-coated coupon (see Fig. 17b), the inner and outer layers are reduced in thickness to 20 and 2 μm, respectively.

Figure 18a shows, as expected, that the oxidation of iron forms a multilayered scale, which consists of a thick (60 μm) wustite inner layer, an intermediate Fe_3O_4 layer (3 μm thick), and a thin (2 μm) Fe_2O_3 outer layer. The most effective coating (strontium) led to the elimination of the outer Fe_2O_3 layer and reduction in the thickness of the FeO and Fe_3O_4 layers, as shown in Fig. 18b.

Thus, iron behaved similarly to cobalt. The outer layers of higher oxides on uncoated cobalt and iron also form by outward cation diffusion, with the cations being produced at the interface with underlying (lower) oxide. For coated samples, inhibition of the interfacial reactions may have occurred.

The appearances of the scale surfaces for the coated and uncoated copper coupons after oxidation at 500°C were identical: compact and small-grained CuO with occasional whiskers. Oxidation of uncoated copper (Fig. 19a) resulted in the formation of an inner (30 μm) Cu_2O layer and an outer (6 μm) layer of CuO. A coating of 250 Å barium provided the greatest reduction in oxidation rate and also prevented scale spallation on cooling as was observed locally for uncoated copper. The scale formed on barium-coated

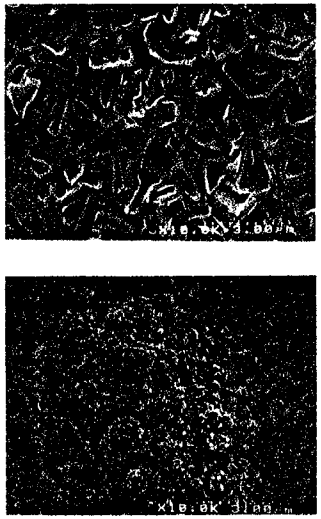

Fig. 16. Scanning electron micrographs of the surface of the scale formed on pure Co coupons after oxidation in 1 atm O_2 at 750°C for 24 h: (a) uncoated Co, (b) Co/250 Å Sr.

copper was nonuniform, as shown in Fig. 19b. The Cu_2O layer thickness ranged from as little as 1 μm up to 28 μm, but the CuO layer remained approximately constant at 5 μm (similar to the uncoated sample). Studies of the oxidation of pure copper have mainly concentrated on the growth of the Cu_2O layer, and the defects and diffusion mechanism in CuO have not been confirmed. Kofstad and Hauffe[39] suggested that the CuO layer grows by outward cation diffusion. Conversely, Valensi[40] suggested that the CuO layer grows by reaction with Cu_2O via inward diffusing oxygen. In the present study, since the outer CuO layer retains a similar thickness for uncoated and coated samples, the consistent explanation would be that of Valensi, because inhibition of the Cu/Cu_2O interfacial step should then lead to a reduction in Cu_2O, but not CuO thickness. The nonuniform nature of the inner Cu_2O layer on coated

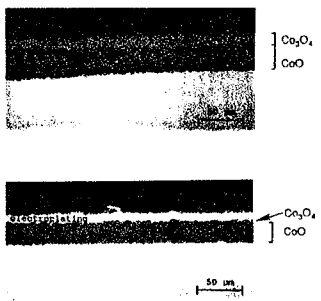

Fig. 17. Optical micrographs of cross sections of oxide scales formed on pure Co coupons after oxidation in 1 atm O_2 at 750°C for 24 h: (a) uncoated Co, (b) Co/250 Å Sr.

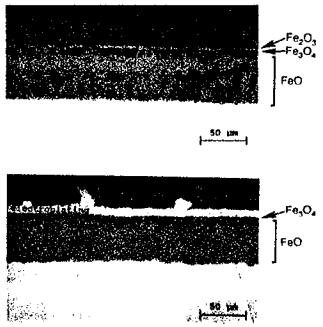

Fig. 18. Optical micrographs of cross sections of oxide scales formed on pure Fe coupons after oxidation in 1 atm O_2 at 600°C for 24 h: (a) uncoated Fe, (b) Fe/250 Å Sr.

copper samples would be explained by a nonuniform provision of segregant at the metal/scale interface.

500 Å films on nickel, cobalt, iron, and copper.—For each of the four pure metals, 500 Å films of the most effective dopants identified for 250 Å depositions were applied, and the oxidation kinetics recorded at 1000°C for nickel, 750°C for cobalt, 600°C for iron, and 500°C for copper. The oxidation kinetics, comparing the uncoated and 250 Å coated samples are shown in Fig. 20 to 23. In every case, the 500 Å coatings were less effective in reducing the oxidation rate than the corresponding 250 Å coatings. For each metal, an optimum deposit thickness was reached between 100 and 500 Å. The fact that 500 Å coatings were less effective than the respective 250 Å coatings confirms that the oxidation inhibition did not result from alkaline earth oxide layers acting as barriers to oxidation, since in this case, 500 Å films would have led to an even greater effect.

General Discussion

For the oxidation of each pure metal coated with a thin film of an alkaline earth metal, the oxidation rate was reduced compared to the respective unmodified surfaces. According to the poisoned-interface model,[5] in the initial stages of substrate oxidation, some of the external alkaline earth oxide particles would be introduced (as markers) into the metal/scale interface, by some initial cation diffusion. The reactive ions (*e.g.*, Ca^{2+}) segregate at interfacial sites

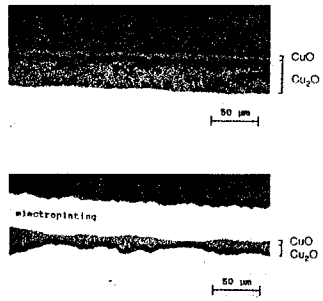

Fig. 19. Optical micrographs of cross sections of oxide scales formed on pure Cu coupons after oxidation in 1 atm O_2 at 500°C for 24 h: (a) uncoated Cu, (b) Cu/250 Å Ba.

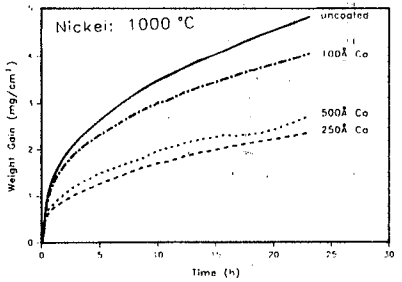

Fig. 20. Weight gain with time for oxidation in 1 atm O_2 at 1000°C of pure Ni coupons with and without 100, 250, and 500 Å coatings of Ca.

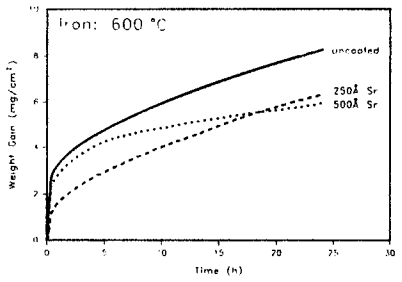

Fig. 22. Weight gain with time for oxidation in 1 atm O_2 at 600°C of pure Fe coupons with and without 250 and 500 Å coatings of Sr.

where they are bound to misfit dislocations, by elastic attraction. The excess surface deposit may be undercut or otherwise interact (by some dissolution and cation diffusion) with the growing scale, but it should not contribute substantially to a change in kinetics or growth mechanism for the scaling reaction. If the interfacial misfit dislocations are totally pinned, so that scale growth must proceed by anion diffusion, then the excess surface deposit would be accumulated (as a marker) near the external scale surface.

The location of the excess impurities would also depend, to some extent on the structure of the initial alkaline earth oxide layer. If oxidation converts the alkaline earth metal films to porous oxide films (likely due to the low volume ratios for conversion of alkaline earth metals to oxides[41]) or cracked oxide films, scale growth by diffusion of cations (at least in the initial stages of oxidation) should not be inhibited, and the impurity oxide would be undercut and incorporated into the scale. Attempts were made to look at the evaporated films (before oxidation) by SEM, but there was insufficient resolution of the deposits, even at high magnification. The location of the reactive elements after oxidation is not presented in this study, but is being carried out by secondary-ion mass spectrometry (SIMS).

For the systems studied here, and also for reactive element additions to chromium or chromia-forming alloys, the relatively large sizes of the impurity ions provide only slight solubilities in the oxide lattices; thus excess impurity would be expected as an oxide phase or segregant in scale grain boundaries (or at the external surface). Besides their lack of significant solubility, the reactive elements of this study exhibit generally the same 2+ valence as the cations for wustite, NiO, and CoO, so the possibility of electrically active lattice doping is negated. For the high temperatures of this study, scale growth on pure nickel, cobalt, iron, and copper is dominantly controlled by lattice diffusion (rather than grain-boundary diffusion). Therefore, although excess alkaline earth should segregate as ions to the grain boundaries in these scales or reside there as oxide phases, they would not introduce an important grain-boundary blocking effect (one popular rationalization for the REE in chromium and chromia-forming alloys). Furthermore, the alkaline earth oxides exhibit cationic point defects and not anionic defects. Thus, BaO, CaO, or SrO at a scale grain boundary would not support inward diffusion of oxygen. For the REE, with chromia, the effective reactive element oxides, *e.g.*, Y_2O_3, ThO_2, and CeO_2, have anion defects and therefore might favor oxygen diffusion.

The extent of oxidation inhibition by the films on each metal was different and correlated somewhat with the thickness of the scales formed. Iron forms a rapidly growing, wustite-dominated scale at 600°C. Iron produced the thickest scales and also showed the least change in oxidation behavior due to the modification. Conversely, the thinnest scales, those formed on nickel at 850°C, showed the most dramatic demonstration of the REE. Indeed, since chromia is a relatively slow-growing oxide, demonstrations of the REE in chromia-formers involve thin scales, on the order of 10 μm or less. A possible explanation of this trend is that the thicker scales may possess a greater area of oxide grain boundaries, leading to the loss of the reactive element from the interface to grain-boundary segregation.

The greatest reduction in rate constant of all the systems studied was a factor of 20, for 250 Å calcium-coated nickel oxidized at 850°C. This degree of inhibition is comparable

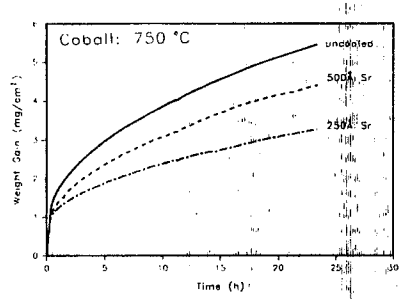

Fig. 21. Weight gain with time for oxidation in 1 atm O_2 at 750°C of pure Co coupons with and without 250 and 500 Å coatings of Sr.

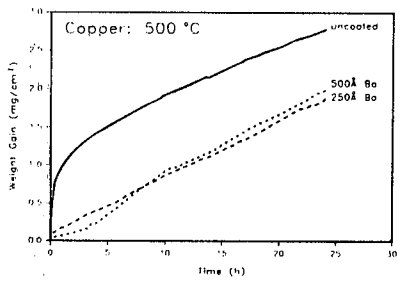

Fig. 23. Weight gain with time for oxidation in 1 atm O_2 at 600°C of pure Cu coupons with and without 250 and 500 Å coatings of Ba.

to the REE for chromia-forming alloys and is thus strong evidence to support the poisoned-interface interpretation[5] of the REE. An improvement in metal/scale adhesion cannot be demonstrated in this system, since the NiO scale formed on pure, uncoated nickel is already very adherent, as are the scales on uncoated cobalt and iron. A noticeable "straightening" of the metal/scale interface was obvious, however, for the coated nickel and cobalt coupons. The oxide scale on uncoated copper tended to spall on cooling, following oxidation at 500°C, and there was some indication that the 250 Å barium (oxide) coating on copper prevented this scale spallation.

The most important characteristic of the full REE is a change in the scale growth mechanism. For the high-temperature oxidations where relatively minor reductions in global scaling kinetics occurred, such a change was not obvious. A change in grain morphology did occur, particularly for coated nickel (at 1000°C) and cobalt (at 750°C) coupons compared to uncoated coupons, including a reduction in oxide grain size, probably caused by the hinderance to grain growth by the dispersed and segregated alkaline earth oxide. However, for a reduction in kinetics by a factor of 20 for the 250 Å calcium (oxide) coating on nickel at 850°C, the scale appearance (Fig. 15c) suggests that there was indeed a change in scale growth mechanism from cation diffusion for the uncoated coupon to anion diffusion for the calcium-coated coupon.

The fourth characteristic of the REE in chromia-formers is the reduced concentration of alloyed chromium needed to produce a continuous, protective chromia scale. Obviously, in the present study of pure metals, this factor does not apply.

In summary, this study has provided some evidence in support of the poisoned-interface explanation of the REE, which suggests that it might be applied to any scaling reaction involving a cation-diffusing scale and a suitable dopant. Chemical analysis of the metal/scale interface to locate the "reactive elements" is needed to support the model further, and some tracer/marker experiments would also be interesting. Of course, the most indisputable evidence would be a demonstration by transmission electron microscopy (or other characterization technique) of reactive-element ions positioned at misfit dislocations at the interface.

Conclusions

1. Deposition by vacuum evaporation of 100, 250, or 500 Å of barium, calcium, and strontium on pure nickel, cobalt, and copper led to substantial reductions in scaling rates compared to uncoated coupons for oxidation at 500 to 1000°C, depending on the substrate.

2. 100 Å films of the alkaline earths led to only localized inhibition of oxidation, due to nonuniform deposition. 250 Å films resulted in the most dramatic effect on the oxidation of the metals, and 500 Å films were less effective.

3. A decrease in temperature (from 1000 to 850°C) resulted in a much a greater effect for a 250 Å coating of calcium on the oxidation of nickel. This reduction in oxidation kinetics at 850°C was greatest for all the systems investigated; the k_p was reduced by a factor of 20 compared to the uncoated nickel.

4. The most effective dopant for each base metal had an ionic radius ratio (R) closest to 1.5, which correlates to the best reactive element ions in chromia-forming alloys.

5. The alkaline earth coatings caused a noticeable change in oxide morphology and relative thickness of layers in multilayered scales.

6. These results provide some preliminary evidence to support the "poisoned-interface" interpretation[5] for the REE. In this model, segregated ions of a specific size pin misfit edge dislocations at the metal/scale interface, which restricts their climb motion required to annihilate vacancies.

Acknowledgments

The authors gratefully acknowledge B. Pieraggi for useful discussions, J. R. Gaines at Superconductive Components Inc. for providing the alkaline earth metals, R. Rokhlin and D. Peterman of the Department of Physics at The Ohio State University for assistance with the vacuum evaporation, funding from U.S. Navy Project 14-92-J-1229, and The Ohio State University Graduate School for provision of a Postdoctoral University Fellowship award which enabled this research to be carried out.

Manuscript submitted Oct. 12, 1993; revised manuscript received Feb. 1, 1994.

The Ohio State University assisted in meeting the publication costs of this article.

REFERENCES

1. D. P. Whittle and J. Stringer, *Philos. Trans. R. Soc. London Ser. A.*, **295**, 309 (1980).
2. D. P. Moon, *Mater. Sci. Technol.*, **5**, 754 (1989).
3. J. Stringer, *Mater. Sci. Eng.*, **A120**, 129 (1989).
4. Y. Saito and B. Onay, *Surf. Coat. Technol.*, **43/44**, 336 (1990).
5. B. Pieraggi and R. A. Rapp, *This Journal*, **140**, 2884 (1993).
6. A. W. Funkenbusch, J. G. Smeggil, and N. S. Bornstein, *Metall. Trans.*, **16A**, 1164 (1985).
7. J. L. Smialek, *ibid.*, **18A**, 164 (1987).
8. K. L. Luthra and C. L. Briant, *Oxid. Met.*, **26**, 397 (1986).
9. K. Przybylski, A. J. Garratt-Reed, and G. J. Yurek, *This Journal*, **135**, 509 (1988).
10. C. M. Cotell, G. J. Yurek, R. J. Hussey, D. F. Mitchell, and M. J. Graham, *Oxid. Met.*, **34**, 173 (1990).
11. B. Pieraggi and R. A. Rapp, *Acta Met.*, **36**, 1281 (1988).
12. J. P. Hirth, B. Pieraggi, and R. A. Rapp, *Oxid. Met.*, Submitted.
13. *Handbook of Chemistry and Physics*, 71st ed., D. R. Lide, Editor, p. 12-1, CRC Press, Boca Raton, FL (1990).
14. J. F. Collins, V. P. Calkins, and J. A. McGurty, Paper presented at ASM-AEC Symposium on the Rare Earths and Related Metals, Chicago, IL, 1959.
15. R. E. Lawn, F. G. Wilson, and C. D. Desforges, *J. Less-Common Met.*, **58**, 107 (1978).
16. V. I. Trefilov, *Dokl. Acad. Nauk.*, **226**, 140 (1976).
17. J. Stringer, A. Z. Hed, G. R. Wallwork, and B. A. Wilcox, *Corros. Sci.*, **12**, 625 (1972).
18. A. Green, *Mater. Sci. Technol.*, **8**, 159 (1992).
19. A. A. Moosa and S. J. Rothman, *Oxid. Met.*, **24**, 133 (1985).
20. D. Loison, J. C. Pivin, J. Chaumont, and C. Roques-Carmes, *Nucle. Instrum. Methods*, **209-210**, 975 (1983).
21. J. M. Hampikian, O. F. Devereux, and D. I. Potter, *Mater. Sci. Eng.*, **A116**, 119 (1989).
22. P. J. George, M. J. Bennett, H. E. Bishop, and G. Dearnaley, *ibid.*, **A116**, 111 (1989).
23. A. T. Chadwick and R. I. Taylor, in *Proceedings of the Ninth International Congress on Metallic Corrosion*, **3**, 381 (1984).
24. D. P. Moon, *Oxid. Met.*, **32**, 47 (1989).
25. N. Nath, N. Eyre, and G. Dearnaley, *Nucl. Instrum. Methods*, **B10/11**, 580 (1985).
26. F. Czerwinski and W. W. Smeltzer, *This Journal*, **140**, 2606 (1993).
27. P. D. Goode, *Inst. Phys. Conf. Ser.*, **28**, 154 (1976).
28. R. A. Collins, S. Muhl, and G. Dearnaley, *J. Phys. F: Metal Phys.*, **9**, 1245 (1979).
29. M. Pons, A. Gallerie, and M. Caillet, *Corros. Sci.*, **23**, 1181 (1983).
30. M. Pons, M. Caillet, and A. Gallerie, *ibid.*, **22**, 239 (1982).
31. Z. Peide, F. H. Stott, R. P. M. Procter, and W. A. Grant, *Oxid. Met.*, **16**, 409 (1981).
32. B. Pieraggi, Private communication.
33. L. Gaudart, P. Renucci, and R. Rivoira, *J. Appl. Phys.*, **49**, 4105 (1978).
34. B. Pieraggi, *Oxid. Met.*, **27**, 177 (1987).
35. R. J. Hussey, P. Papaiavocou, J. Shen, D. F. Mitchell, and M. J. Graham, *Mater. Sci. Eng.*, **A120**, 147 (1989).
36. B. A. Pint and L. W. Hobbs, Abstract 1186, p. 1711, The Electrochemical Society Extended Abstracts, Vol. 93-1, Honolulu, HI, Meeting of the Society, May 16-21, 1993.
37. W. Laqua and H. Schmalzried, in *High-Temperature Corrosion*, R. A. Rapp, Editor, p. 115, Conf. Proc. NACE-6, San Diego, CA, March 2-6, 1981, NACE (1983).
38. K. Hauffe and P. Kofstad, *Z. Elektrochem.*, **59**, 399 (1955).
39. G. Valensi in Proceedings of Pittsburgh International Conference on *Surface Reactions*, p. 146, Corrosion Publ. Co., Pittsburgh, PA (1948).
40. N. B. Pilling and R. E. Bedworth, *J. Inst. Met.*, **29**, 529 (1923).

Electrochemical Behavior of Lithium Electrolytes Based on New Polyether Networks

F. Alloin, J-Y. Sanchez, and M. Armand

Laboratoire d'Ionique et d'Electrochimie du Solide CNRS, Domaine Universitaire, BP75 38402 Saint-Martin d'Hères Cedex, France

ABSTRACT

New polyethers have been prepared from polycondensation between several α, ω-dihydroxy(oxyethylene) and 3-chloro-2-chloromethyl-1-propene (CCMP). The CCMP units decrease both the crystallinity content and the melting point of the polyether chains. The free-radical polymerization of the dangling double bonds decreases the melting point of the crystalline phase and greatly enhances the mechanical strength of the network. The conductivity as well as the thermal behavior and the electrochemical stability of lithium electrolytes based on these networks have been investigated. Conductivity values close to 10^{-5} S · cm^{-1} at 20°C were obtained for some salt concentrations without compromising the electrochemical stability. A transport number $t_+ = 0.46$ has been determined for LiTFSI/network complexes.

The use of polymer electrolytes in electrochemical devices such as primary and secondary batteries and in electrochromic windows has opened new opportunities. The lifetime of secondary batteries using lithium anodes has been markedly enhanced by replacing liquid organic solvents based on ethylene or propylene carbonate by a polymeric solvent. Over 1000 deep discharge cycles (100% depth of discharge) have been demonstrated for a thin film configuration.[1] Furthermore, the use of an all solid-state construction guarantees the safety of the battery as established from tests performed at Hydro-Quebec: short-circuits on 10 Wh cells which brought the core of the cells to a temperature above the melting point of the lithium without the onset of an exothermic reaction followed by a rapid decrease of the cell temperature.[1]

Although the state-of-the-art polymer electrolyte batteries working in the 50 to 80° temperature range are perfectly acceptable for electric vehicles, it would be interesting to increase the ambient temperature conductivity of the polymer electrolyte. As ^{7}Li nuclear magnetic resonance (NMR) performed on semicrystalline poly(oxyethylene) complexes with lithium salts has established the prevalence of the ionic conductivity in the amorphous phase,[2] several attempts to diminish or suppress the crystallinity have been made over the past years. For instance, solvating chains arranged in a network through urethane linkage[3] or comb polymers with a siloxane backbone[4] remain completely amorphous at room temperature. Nevertheless the lifetime of lithium batteries is related to the electrochemical stability of the polymer electrolyte especially in contact with lithium metal at the negative electrode, and the stability of urethane or siloxane links is questionable. Up to now, only carbon-oxygen single bonds have been shown to have enough long term stability *vs.* lithium for battery operation.

Another way to reduce the crystallinity of the solvating host polymer is to use oxymethylene linked polyethers prepared[5-7] by a simple Williamson condensation reaction. This elegant and inexpensive route produces polymers which are amorphous at room temperature when starting from α, ω-dihydroxy oligo(oxyethylene): PEG400 or PEG600. Therefore the lithium polymer electrolytes prepared from these polycondensates exhibit high conductivity at ambient temperature. Furthermore the acetal link between the oligoether blocks is stable *vs.* lithium as demonstrated by the electrochemical studies of polydioxolane.[8,9] Although these polymers have undeniable advantages, they also have some drawbacks: (*i*) The condensation reaction gives samples with a broad molecular weight distribution which complicates the purification especially since the average molecular weights are rather low. (*ii*) The polymer electrolytes have poor mechanical properties and are difficult to process in thin films. In order to overcome this problem Wilson *et al.* have prepared block copolymers containing a hard segment.[10] (*iii*) Due to the high sensitivity[11] of the acetal link to acids, depolymerization reaction could easily take place, compromising its production on an industrial scale during the purification process. Also, many intercalation oxides possess highly acidic surface groups (VO_x, . . .) which would cleave the polymer contained in the composite electrode.

Along the same line, we have investigated[12] the polycondensation of several α, ω-dihydroxy oligo(oxyethylene) with unsaturated dihalogeno compounds such as 3-chloro-2-chloromethyl-1-propene and 1,4-dibromo-2-butene. Details of the synthesis and polycondensation mechanisms will be published elsewhere.[13] The main advantages of this synthesis lie in the chemical stability of the ether link (compared to that of acetal) as well as in the possibility to cross-link the resulting polycondensates by free-radical initiation.